

# **Enhanced ionic conductivity in poly(vinylidene fluoride) electrospun separator membranes blended with different ionic liquids for lithium ion batteries**

J. C. Barbosa<sup>1,2</sup>, D.M. Correia<sup>1,2</sup>, R. Gonçalves<sup>3</sup>, V. de Zea Bermudez<sup>2</sup>, M.M. Silva<sup>3</sup>, S. Lancers-Mendez<sup>4,5\*</sup> and C. M. Costa<sup>1,3\*</sup>

<sup>1</sup>Center of Physics, University of Minho, 4710-058 Braga, Portugal

<sup>2</sup>Department of Chemistry and CQ-VR, University of Trás-os-Montes e Alto Douro, 5000-801 Vila Real, Portugal

<sup>3</sup>Center of Chemistry, University of Minho, 4710-058 Braga, Portugal

<sup>4</sup>BCMaterials, Basque Center for Materials, Applications and Nanostructures, UPV/EHU Science Park, 48940 Leioa, Spain.

<sup>5</sup>Ikerbasque, Basque Foundation for Science, 48013 Bilbao, Spain

**\*Corresponding Authors** Email: S. Lancers-Méndez  
[senentxu.lancers@bcmaterials.net](mailto:senentxu.lancers@bcmaterials.net) and C. M. Costa ([cmscosta@fisica.uminho.pt](mailto:cmscosta@fisica.uminho.pt));

**Abstract:**

Electrospun poly(vinylidene fluoride) (PVDF) fiber membranes doped with different ionic liquids (ILs) and sharing the same anion were produced and their potential as separator membranes for battery applications was evaluated. Different types of ILs containing the same anion, bis(trifluoromethylsulfonyl)imide [TFSI]<sup>-</sup>, were used with IL concentrations ranging between 0 and 15 wt.%. The morphology, microstructure, thermal and electrical properties (ionic conductivity and electrochemical window) of the membranes were evaluated. The presence of ILs in the PVDF polymer matrix influences the fiber diameter and the content of the polar  $\beta$  phase within the polymer, as well as the degree of crystallinity. The thermal stability of the membranes decreases with the incorporation of IL. Impedance spectroscopy tests show a maximum ionic conductivity of  $2.8 \text{ mS.cm}^{-1}$  for 15% of 1-ethyl-3-methylimidazolium bis(trifluoromethylsulfonyl)imide ([Emim][TFSI]) at room temperature. The electrochemical stability of the samples ranges from 0.0 to 6.0 V. When evaluated as battery separator membranes in C-LiFePO<sub>4</sub> half-cells, a maximum discharge capacity of  $119 \text{ mAh.g}^{-1}$  at C-rate was obtained for the PVDF membrane with 15% [Emim][TFSI], with a coulombic efficiency close to 100%. The results demonstrate that the produced electrospun membranes are suitable for applications as separators for lithium ion batteries (LIBs).

**Keywords:** Ionic liquids, electrospinning, PVDF, separators

## 1. Introduction

Since the industrial revolution, a continuous growth in world energy demand has been observed. In an economy dependent on the consumption of fossil fuels, such as oil and coal, the growing demand for energy also increases the pressure on the environment, with a continuous extraction of non-renewable natural resources, impacts on the climate and problems associated with greenhouse gases emissions [1]. Hence, a transition to a sustainable development, based on cleaner and renewable energy resources to decarbonize the economic system is needed. However, as renewable energies do not guarantee a permanent supply of power into the grids, complementary systems allowing the storage of energy in hours of high production, to be used later, whenever needed, are sought [2].

Lithium ion batteries (LIBs) are widely used to power mobile devices, such as smartphones, laptops or electric vehicles, mainly due to their high energy density and long cycle life [3]. A typical LIB is composed by two electrodes (anode, negative electrode and cathode, positive electrode) and a separator/electrolyte [4].

The separator/electrolyte is therefore a key component in LIBs. The separator is placed between the electrodes, preventing their physical contact, avoiding short circuits and allowing the flow of ions between them. Its ideal properties are high ionic conductivity and chemical stability, high wettability and excellent mechanical strength [5]. Some of the most used materials in separators are poly(ethylene oxide) (PEO) [6-9], poly(acrylonitrile) (PAN) [8, 10, 11] and poly(vinylidene fluoride) (PVDF) and its copolymers [10, 12-14].

PVDF is an electroactive polymer suitable for application in energy storage devices, due to its non-toxicity, mechanical stability, high dielectric constant and dipolar moment, and the ability to be processed in a wide variety of forms and shapes [15]. However, this

material does not meet all the desired properties of battery separators. Consequently, the addition of electrolytes is essential to facilitate the ion flow, increasing the ionic conductivity. Another valid approach is the addition of fillers into the polymeric matrix to enhance the ionic conductivity without the requirement to introduce liquid components that hinder both the safety and the cycle life of the LIB. Some well-studied fillers are silicon dioxide ( $\text{SiO}_2$ ) [16], aluminum oxide ( $\text{Al}_2\text{O}_3$ ) [17] and ionic liquids (ILs) [18-20]. ILs are defined as salts with melting temperatures below 100 °C. Their high ionic conductivity and non-volatility make them excellent candidates as fillers in LIBs, as organic solvents or electrolytes [21]. Several experimental techniques can be used to produce membranes with ILs, including solvent casting [22], doctor blade [23], hot pressing [24] and electrospinning [25].

Electrospinning involves the application of a high voltage to a polymer solution to form nonwoven fibers. It is a simple, low-cost, efficient and highly reproducible technique, successfully employed in a wide range of applications [26, 27], with special relevance in separators for battery application in the form of monolayer, multilayer, composite, surface modified, and gel polymer electrolytes [28].

Typically, electrospun composite membranes are based on different polymer matrices, being polyimide (PI) [29], poly(acrylonitrile) (PAN) [30] and PVDF [31] the most used. For these polymer matrices, the most studied fillers are  $\text{SiO}_2$  [32], titanium dioxide ( $\text{TiO}_2$ ) [33],  $\text{Al}_2\text{O}_3$  [34], lithium lanthanum titania (LLTO) [35] and lithium aluminum titanium phosphate (LATP) [36]. Electrospinning has been used to obtain fiber membranes based on poly(ethylene)/ $\text{SiO}_2$  composite membranes with suitable electrochemical properties [37-39].  $\text{SiO}_2$  nanoparticles were also dispersed in a poly(vinylidene fluoride)-co-hexafluoropropylene (PVDF-HFP) matrix. The addition of ILs into these membranes allows the formation of a gel polymer electrolyte with improved safety and cycling

stability for lithium sulfur batteries [40], and LIBs [41]. ILs are still not well studied as fillers. Just one study has been reported, in which the use of 1-butyl-3-methylimidazolium bis(trifluoromethanesulfonyl)imide ([Bmim][TFSI]) allowed high electrochemical stability, wettability and battery performance [42]. ILs are also utilized as electrolytes, where electrospun PAN membranes using ILs as electrolyte presented higher porosity and wettability than commercial Celgard® separators, as well as suitable mechanical properties. They also showed high cycling stability and discharge capacity at all tested rates [43]. The addition of 1-propyl-1-methyl piperidinium bis(trifluoromethanesulfonyl)imide ([Pmpip][TFSI]) into an electrospun PVDF-HFP gel polymer electrolyte matrix proved to suppress the lithium dendrite formation in LIBs and showed high electrolyte uptake and lithium transference number [44].

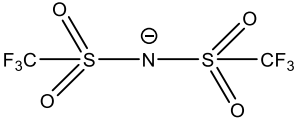
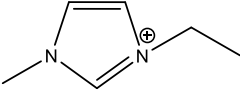
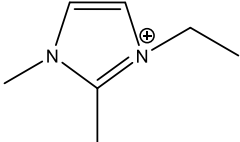
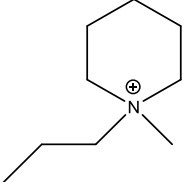
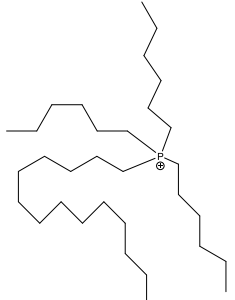
Despite these interesting works, there is still a lack of systematic knowledge that allows the proper selection of ILs in order to improve the membrane performance for battery applications. Thus, the objective of this work is to understand the effects of different ILs sharing the same anion, on separator membrane conductivity and battery performance, in order to optimize separator membranes for LIB applications. This study reports on the production of electrospun separator membranes based on PVDF and ILs sharing the same anion, [TFSI]<sup>-</sup>, but different cations (trihexyl(tetradecyl)phosphonium [P66614]<sup>+</sup>, 1-methyl-1-propylpiperidinium [Pmpip]<sup>+</sup>, 1-ethyl-3-methylimidazolium [Emim]<sup>+</sup>, 1-ethyl-3-dimethylimidazolium [Edmim]<sup>+</sup>) and different amounts of [Emim][TFSI]. The effect of the ILs on the PVDF membrane microstructure, thermal stability and ionic conductivity were evaluated. In addition, the battery performance incorporating these membranes is presented.

## 2. Experimental

### 2.1. Materials

Poly(vinylidene fluoride) (PVDF, Solef 5130) and N, N-dimethyl formamide (DMF, 99%) were purchased from Solvay and Merck, respectively. N,N'-dimethylpropyleneurea (DMPU, 99%) and 1 M LiPF<sub>6</sub> in ethylene carbonate-dimethyl carbonate (EC-DMC, 1:1 vol) were purchased from LaborSpirit and Solvionic, respectively. For the electrospun composites, the different ILs share the same anion, [TFSI]<sup>-</sup>, as it is widely used in battery applications due to its electrochemical stability, low volatility and high thermal stability [45]. The selected ILs were purchased from Iolitec (>99%) and present different ionic conductivity and viscosity values, affecting the membrane final characteristics. The most relevant properties of the selected ILs are shown in Table 1.

**Table 1** - ILs types used and their characteristics. Data obtained from the provider.

Anion	Cation	Ionic conductivity (mS cm <sup>-1</sup> )	Viscosity (mPa s <sup>-1</sup> )
	[Emim] <sup>+</sup> 	6.63	39.4
	[Edmim] <sup>+</sup> 	3.18	68.5
	[Pmpip] <sup>+</sup> 	2.12	176
	[P66614] <sup>+</sup> 	0.14	304

## 2.2. Electrospun membranes preparation

PVDF and PVDF/IL fibers were processed by electrospinning, following the general guidelines presented in [46]. In short, a 15 wt.% solution of PVDF in DMF was prepared under magnetic stirring at room temperature until the complete polymer dissolution. For PVDF/[Emim][TFSI] fibers, prior to polymer dissolution, different amounts of 5, 10 and 15 wt.% [Emim][TFSI] IL, relative to the polymer, were dispersed in the DMF. For the other ILs, 15 wt.% IL content was used. Then, the polymeric solution was placed in a plastic syringe (10 mL) equipped with a steel needle with an inner diameter of 0.5 mm. After an optimization procedure, the process was conducted at 15 kV with a high voltage power supply from Glassman (model PS/FC30P04) with a solution feed rate of 0.2 mL.h<sup>-1</sup> with a syringe pump. The electrospun fibers were collected on an aluminum plate. The viscosity of the solutions was between 1.54 and 3.97 Pa.s for 340 to 26.9 s<sup>-1</sup>.

## 2.3. Characterization techniques

For the morphological analysis, the PVDF and PVDF/IL electrospun fibers have been covered with a thin gold layer by sputter coating (Polaron, model SC502) and the morphology was investigated with a scanning electron microscope (SEM) (FEI NOVA 200). The distribution and fiber average diameter were calculated on at least 30 fibers using the SEM micrographs and the ImageJ software.

Attenuated total reflection Fourier transform infrared spectroscopy (ATR-FTIR) was carried out with a JASCO FT/IR- 4100, using 32 scans with a resolution of 4 cm<sup>-1</sup>. Thermal analysis of the samples was evaluated by differential scanning calorimetry (DSC) measurements (Mettler Toledo DSC822e) between 20 to 200 °C at a scan rate of 10 °C min<sup>-1</sup>. The experiments were carried out under nitrogen purge and the obtained data were standardized for the weight of the polymer. The thermal degradation was evaluated by thermogravimetry under a nitrogen flow rate of 50 mL.min<sup>-1</sup>. Measurements were

performed between 25 and 900 °C at a heating rate of 10 °C.min<sup>-1</sup> in a Pyris1TGA, Perkin-Elmer set-up.

## 2.4. Electrochemical performance

### 2.4.1. Ionic conductivity and cyclic voltammetry

The ionic conductivity value of the membranes, placed between gold electrodes, was measured by impedance analyses on an Autolab PGSTAT-12 (Eco Chemie) at frequencies between 500 mHz and 65 kHz and temperatures from 20 to 140 °C (Buchi TO 50 oven). Ionic conductivity ( $\sigma$ ) was determined by:

$$\sigma = \frac{t}{A \cdot R_b} \quad (1)$$

where  $t$  is the thickness,  $A$  is the area and  $R_b$  is the membrane bulk resistivity, obtained by the interception of the minimum value of  $Z''$  with the slanted line in the real impedance ( $Z'$ ).

The electrochemical stability of the membranes was evaluated by cyclic voltammetry, carried out within a dry argon-filled glovebox through the Autolab PGSTAT-12 (Eco Chemie) at a scan rate of 10 mV.s<sup>-1</sup> using a two-electrode cell configuration with a gold microelectrode as working electrode [47].

### 2.4.2. Battery preparation and cycling tests

The cathode was prepared using 80 wt.% of lithium iron phosphate C-LiFePO<sub>4</sub> as active material, 10 wt.% of carbon black as conductive material and 10 wt.% of poly(vinylidene fluoride), PVDF as a binder in 2.25 mL of DMPU solvent to 1g of solid material. More details about the electrode preparation are reported in [48]. The resulting slurry was then casted into aluminum foil by doctor-blade technique and dried at 100 °C for 2 h. The active mass loading was ~ 1.5 mg.cm<sup>-2</sup>.



Swagelok type Li/C-LiFePO<sub>4</sub> half-cells were assembled in an argon-filled glove box and prepared using electrospun membranes as separator (10 mm diameter) soaked in electrolyte solution – 1M LiPF<sub>6</sub> in EC: DMC. Metallic lithium (8 mm diameter) was used as the anode and the C-LiFePO<sub>4</sub> based electrode as cathode (8 mm diameter). The charge-discharge tests were evaluated at room temperature in the voltage range of 2.5 V to 4.2 V at current rates of C/8 to 2C (C = 170 mAh.g<sup>-1</sup>), using a Landt CT2001A Instrument. The electrical properties of Li/C-LiFePO<sub>4</sub> half-cells with IL before and after cycling were evaluated by electrochemical impedance spectroscopy (EIS) with an Autolab PGSTAT12 instrument, in the frequency range from 1 MHz to 10 mHz, with an amplitude of 10 mV.

### **3. Results and discussion**

#### *3.1. Electrospun fiber membranes morphology*

Pristine PVDF and PVDF/IL comprising different IL cations were electrospun into fibers by electrospinning. Figure 1a shows the highly porous PVDF electrospun membrane with a smooth surface. Analogous results are observed for samples containing different ILs (Figure 1b-1c). Independently of the IL cation, the incorporation of IL led to a decrease in fiber diameter (Figure 1d), from ~250 μm for pristine PVDF to ~180 μm for fibers with different contents of [Emim][TFSI]. No significant changes were observed with increasing IL content from 5 to 15 wt.%. However, the fiber diameter increases with increasing alkyl cation chain length for an IL content of 15 wt.%. Similar fiber diameters were observed for the PVDF/[Pmpip][TFSI] and PVDF/[P66614][TFSI] fibers. The parameters that most influence the fiber diameter in the present case are associated with the electrical solution conductivity and the solution viscosity. The observed decrease in the fiber diameters is mainly related to the presence of the ionic charges of the different ILs, which promote a higher stretching of the solution jet when compared to pristine PVDF [49]. In this case, the effect of viscosity, with small variations for different

solutions, on the final size of the fibers is negligible when compared to the presence of the ionic charges. This decrease in fiber diameter is more marked for PVDF/IL fibers containing the imidazolium cations due to the highest ionic conductivity of these ILs [50].

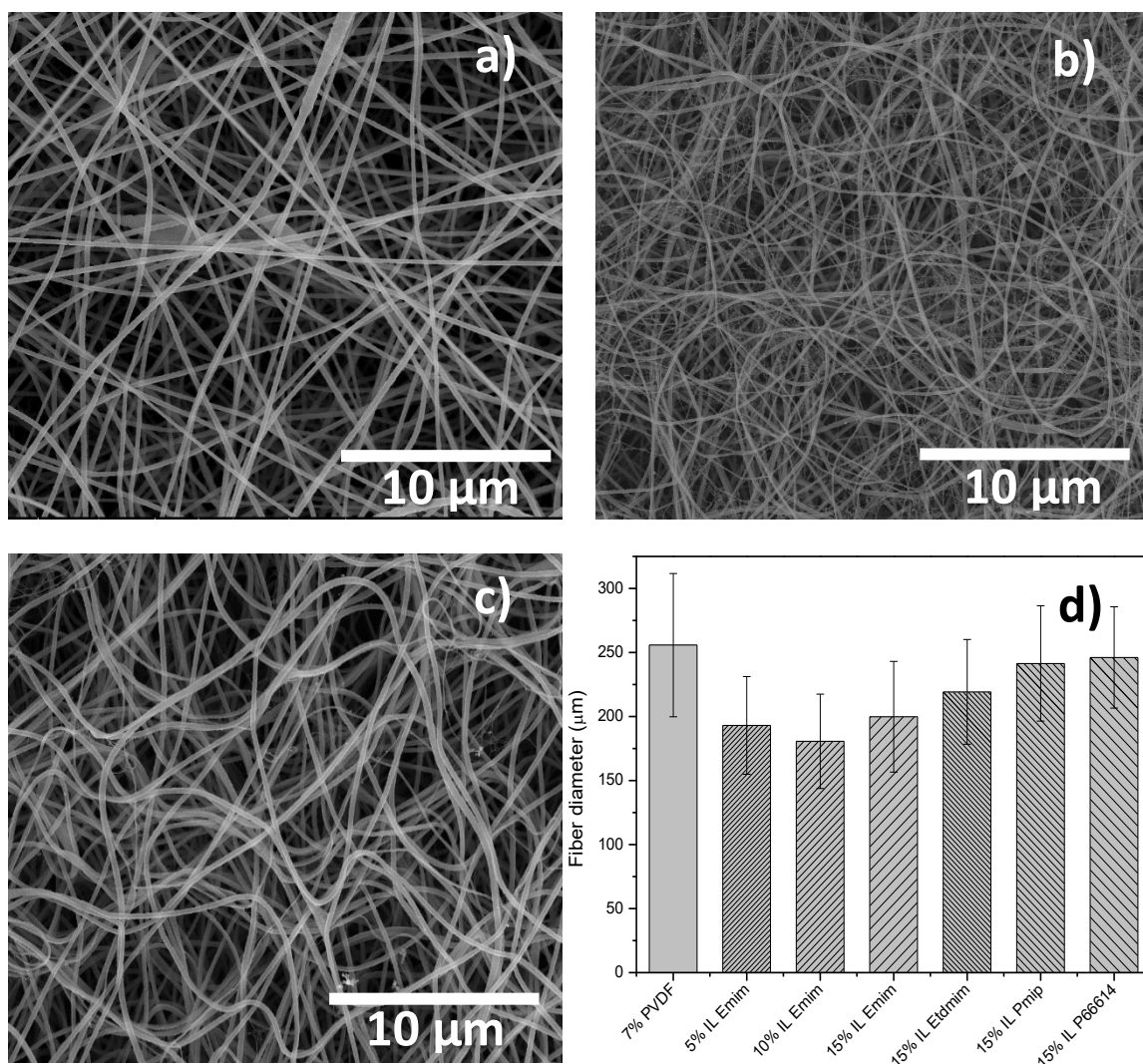


**Figure 1** - SEM images of electrospun a) pristine PVDF and PVDF/IL membranes containing different contents of [Emim][TFSI]: b) 15 wt.%, c) 15 wt.% [Pmpip][TFSI] and d) average fiber diameter for the different PVDF and PVDF/IL fibers.

### 3.2. Physical-chemical properties

#### 3.2.1. Polymer phase

In order to evaluate the effect of IL incorporation on the chemical structure of the PVDF and the influence of the different ILs on the PVDF polymer phase, the ATR-FTIR spectra were recorded (Figure 2a).

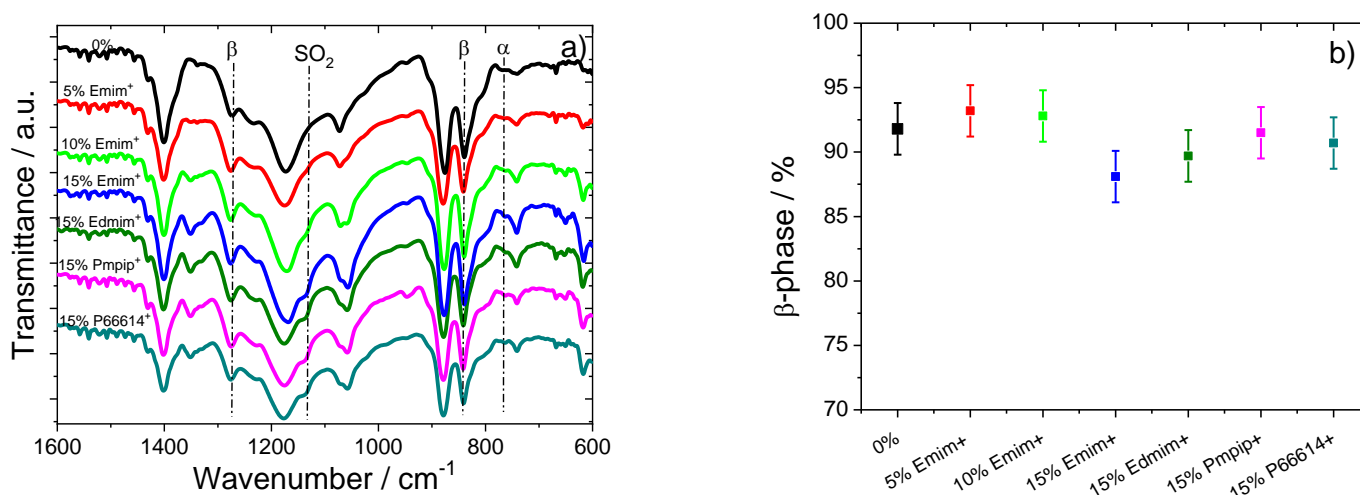


**Figure 2** - a) ATR-FTIR spectra of the PVDF and PVDF/IL electrospun fibers and b) quantification of the electroactive  $\beta$  phase content of the different samples.

Figure 2a shows that the main characteristic absorption bands of PVDF are presented in the ATR-FTIR spectra, independently of the IL type and content. The CF<sub>2</sub> and CH<sub>2</sub> characteristic absorption bands of PVDF are observed approximately at 795, 766, 678 and 976 cm<sup>-1</sup> [51, 52]. These absorption bands are indicative of the presence of the PVDF  $\alpha$  phase. The absorption bands indicative of the presence of the electroactive  $\beta$  phase, associated with the stretching vibration of the CH<sub>2</sub> group, are observed at 840, 879, 1071, 1176, 1275 and 1402 cm<sup>-1</sup> [51, 52]. The weak absorption band observed at 1232 cm<sup>-1</sup> is attributed to the PVDF  $\gamma$  phase [51].

Upon incorporation of the different ILs, no changes in the PVDF chemical structure occurred. For PVDF/IL composites, the absorption bands of the IL anion [TFSI]<sup>-</sup> are identified: the absorption band at 740 cm<sup>-1</sup> ascribed to the cis [TFSI]<sup>-</sup> conformation and

the asymmetric and symmetric stretching vibration modes characteristic of the SO<sub>2</sub> group at 1132 and 1349 cm<sup>-1</sup> [53]. The absorption bands at 612, 1051 and 1479 cm<sup>-1</sup>, attributed to the stretching vibration mode of SO<sub>2</sub> group, to the asymmetrical S–N–S stretching mode, and to the C–H bending of methyl group, respectively, are overlapped with those of PVDF [54].

Assuming that there is not  $\gamma$  phase, the electroactive  $\beta$  phase present in the PVDF and PVDF/IL fibers was quantified from the ATR-FTIR spectra using equation 2 [51]:

$$F(\beta) = \frac{X_{\beta}}{X_{\alpha} + X_{\beta}} = \frac{A_{\beta}}{(K_{\beta} / K_{\alpha})A_{\alpha} + A_{\beta}} \quad (2)$$

where,  $F(\beta)$  represents the  $\beta$  phase content;  $A_{\alpha}$  and  $A_{\beta}$  the absorbances at 766 and 840 cm<sup>-1</sup> that corresponds to the  $\alpha$  and  $\beta$  phases material;  $K_{\alpha}$  and  $K_{\beta}$  are the absorption coefficients at the respective wave number and  $X_{\alpha}$  and  $X_{\beta}$  the degree of crystallinity of each phase. The value of  $K_{\alpha}$  is  $6.1 \times 10^4$  and the value of  $K_{\beta}$  is  $7.7 \times 10^4$  cm<sup>2</sup>.mol<sup>-1</sup> [51].

Figure 2b shows the electroactive  $\beta$  phase content for the PVDF and PVDF/IL electrospun fibers. The PVDF fibers present a high  $\beta$  phase content mainly due to the room temperature processing, which promotes the PVDF crystallization in  $\beta$  phase. Upon addition of [Emim][TFSI] to the polymer solution, the  $\beta$  phase content remained almost constant, with variation within the experimental error, after the IL content was increased from 5 to 10 wt.%. The higher  $\beta$  phase content for electrospun membranes, after comparison with PVDF/IL films [50], is indicative that during the electrospinning process and together with the effect of room temperature solvent evaporation [46], the electrostatic interactions between the IL and the strong dipolar moment of the polymer further promotes the orientation of the CH<sub>2</sub>-CF<sub>2</sub> dipoles in the  $\beta$  phase “trans-planar” zig-zag characteristic conformation. Independently of the IL type, the  $\beta$  phase content remains nearly constant with the incorporation of 15 wt.% of IL within the PVDF matrix,

with PVDF/[Emim][TFSI] presenting the lowest  $\beta$  phase value (88%), when compared to the other electrospun membranes (~91%). From Figure 2b it is also possible to conclude that the electrostatic interactions between IL and PVDF are favored by an increase in the alkyl IL chain, as observed for the [Emim]<sup>+</sup> and [Edmim]<sup>+</sup> cations. The higher  $\beta$ -phase content in the polymer leads to a higher polarity that will enhance the lithium ion migration within the separator [55].

### 3.2.2. Thermal and mechanical properties

The thermal properties of the electrospun fibers were determined by DSC measurements, in order to detect possible modifications in the thermal stability and melting behavior of the PVDF after the IL incorporation. The DSC curves for the pristine PVDF and PVDF/IL membranes, presented in Figure 3a, show that there were no significant changes in the melting peak of PVDF (~160°C) after the incorporation of the different ILs types and content. Only a broader melting peak is observed for samples containing different IL cations ([Pmpip]<sup>+</sup> and [P66614]<sup>+</sup>). It is also observed that the melting peak area decreases for all PVDF/IL electrospun fibers compared to pristine PVDF, an indication of a decrease in the degree of crystallinity of the polymer because of the hindering of the crystallization process due to the IL-polymer chain electrostatic interactions [50].

The degree of crystallinity ( $\Delta X_c$ ) of the PVDF and PVDF/IL electrospun fibers was calculated using the Equation 3 [51]:

$$\Delta X_c = \frac{\Delta H_s}{x\Delta H_\alpha + y\Delta H_\beta} \quad (3)$$

where  $\Delta H_s$  represents the melting enthalpy of the sample and  $\Delta H_\alpha$  (93.07 J.g<sup>-1</sup>) and  $\Delta H_\beta$  (103.4 J.g<sup>-1</sup>) are the melting enthalpies of a 100% crystalline  $\alpha$  and  $\beta$  PVDF sample, respectively.  $x$  and  $y$  represent the fraction of  $\alpha$  and  $\beta$  phase present in the sample.

Figure 3b shows that the degree of crystallinity decreased upon IL incorporation within the polymer matrix. For the electrospun fibers containing different [Emim][TFSI] amounts, the degree of crystallinity decreased from ~62 to 42 % for increasing IL content from 5 to 15 wt.%, respectively. No significant changes occur between electrospun fibers containing imidazolium cations with different size ([Emim]<sup>+</sup> and [Edmim]<sup>+</sup>) and cations nature ([Pmpip]<sup>+</sup> and [P66614]<sup>+</sup>). Thus, these results are an indication that for the different electrospun fibers, the IL-polymer interaction hindered polymer crystallization process and promoted defects around the IL sites in the lamellae of the spherulites.

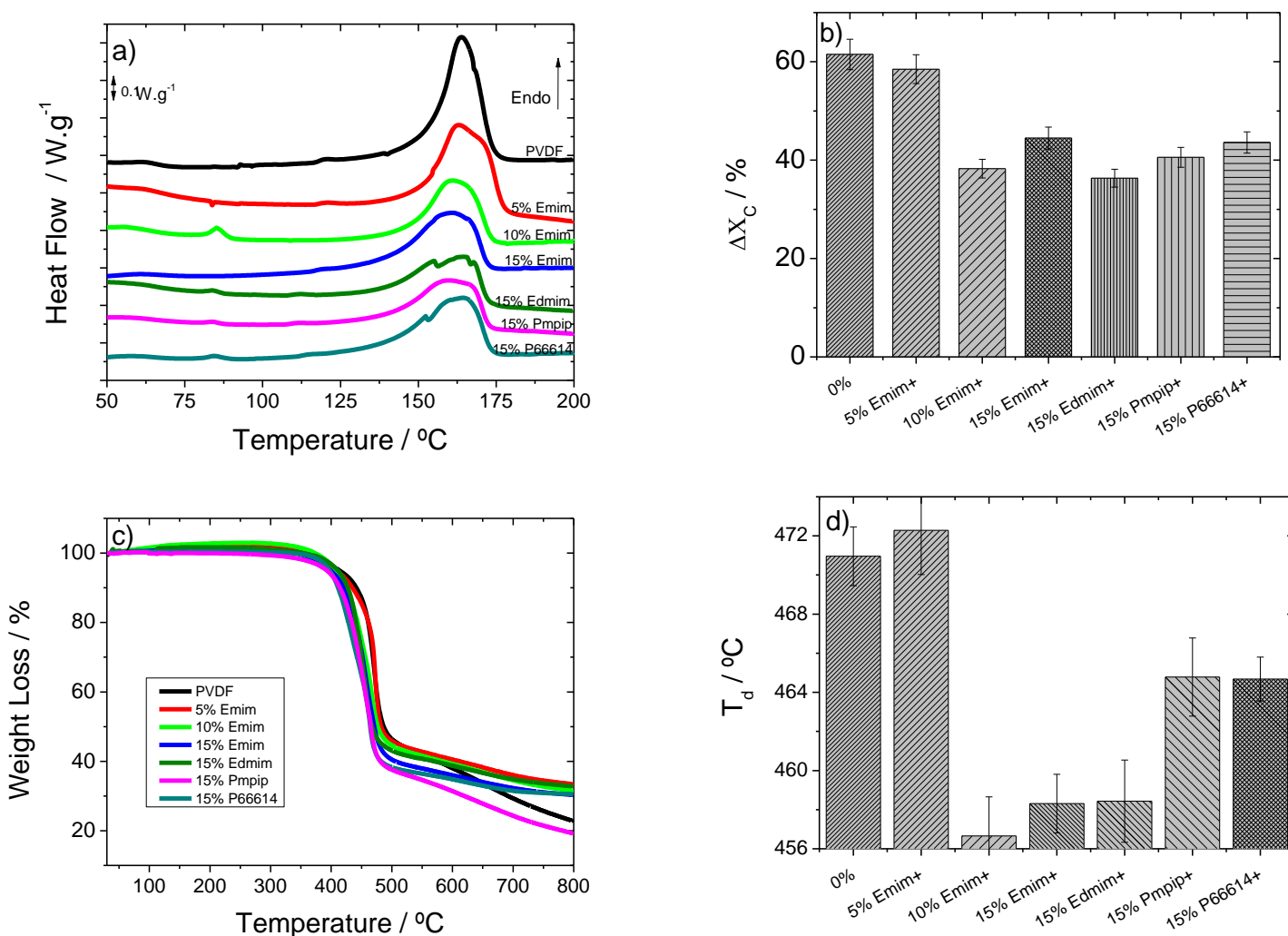


**Figure 3** - a) DSC thermograms, b) degree of crystallinity, c) thermal degradation measurements and d) thermal decomposition temperature (T<sub>d</sub>) for the different PVDF and PVDF/IL electrospun fiber mats.

The influence of IL content and nature on the thermal stability of electrospun fibers was studied by thermogravimetric analysis (TGA). The TGA curves for the different pristine PVDF and PVDF/IL electrospun membranes are shown in Figure 3c. All membranes are characterized by a single thermal degradation process related to the thermal decomposition of the  $-\text{CH}_2\text{-CF}_2-$  groups of the PVDF polymer chain [50], with an onset temperature ( $T_{\text{onset}}$ ) (determined by initial point of the degradation step) at  $\sim 450$  °C for pristine PVDF.

Independently of the IL content and cation nature, the thermal stability of the PVDF/IL electrospun fibers decreased upon IL content incorporation. Figure 3c shows a decrease in the thermal stability, by shifting to a lower degradation temperature, with an increase of [Emim][TFSI] content ( $T_{\text{onset}}$  [Emim 5%]<sup>+</sup>  $\sim 426$  °C, [Emim 10%]<sup>+</sup>  $\sim 418$  °C and [Emim 15%]<sup>+</sup>  $\sim 411$  °C). The highest decrease in thermal stability was observed for the PVDF/[Edmim][TFSI] fibers ( $T_{\text{onset}} \sim 395$  °C). This decrease in the thermal stability of the PVDF/IL membranes results from the ILs interaction with the fluorinated polymer matrix, which promotes a destabilization of the PVDF polymer structure [49].

Figure 3d shows the decomposition temperature ( $T_d$ ) of the different samples calculated as the point of maximum derivative. The decomposition temperature of pristine PVDF occurs at 471 °C, being observed a decrease in the decomposition temperature with the addition of different ILs types and contents. In PVDF/[Emim][TFSI] membranes with 5 wt.% IL content, this effect is not significant due to the low IL content, but increasing the IL content up to 15 wt.%, the decomposition temperature decreases down to 458 °C.

All membranes with the same content of different imidazolium cations ([Emim]<sup>+</sup> and [Edmim]<sup>+</sup>) show the same decomposition temperature, suggesting that the cation size has no influence in the thermal degradation of PVDF. Furthermore, samples with ILs of different nature ([Pmpip]<sup>+</sup> and [P66614]<sup>+</sup>) also show the same decomposition

temperature, but higher than those of the ILs mentioned above for the same IL content. Thus, ILs with different nature allow tuning the degradation temperature of PVDF through varying IL-polymer chain electrostatic interactions [50].

The mechanical properties of the electrospun membranes were evaluated in pristine PVDF with and without electrolyte, as presented in Figure S1 in the supplementary information. The IL addition influences the PVDF polymer structure to induce a plasticizing effect [50]. Since the prepared samples present a low IL amount percentage (up to 15%), the mechanical properties show for the different samples a similar response to that shown in Figure S1. The incorporation of the electrolyte solution decreases the Young Modulus of the PVDF electrospun fibers from 17 to 3 MPa. It is observed that the addition of the electrolyte solution maintains the samples mechanically suitable (>1 MPa) [56] for being used as separator in LIBs.

### *3.3. Ionic conductivity and electrochemical stability*

The ionic conductivity values of the different electrospun membranes were determined by electrochemical impedance spectroscopy (EIS).

Figure 4a shows the ionic conductivity value (calculated by equation 1) as a function of temperature, calculated through the Nyquist plot (real impedance -  $Z'$  - vs imaginary impedance -  $Z''$ ) from the interception at high-frequency with the real axis (Nyquist plots are shown as supplementary information, Figure S2). For the pristine PVDF and PVDF/IL membranes doped with an [Emim][TFSI] content up to 10 wt.%, the Nyquist plots at lower temperatures (data not shown) are characterized by three different regions: a semi-circle located at the high frequency range, that corresponds to a charge transfer process, a straight line at lower frequencies, characteristic of charge diffusion processes, and finally, the transition between these two phenomena [57]. For higher IL contents (15 wt.%), the Nyquist plots of the samples are characterized by a straight line for the whole



frequency range resulted from high ionic conduction (data not showed) [58]. As represented in figure 4a, the ionic conductivity increases with increasing temperature and IL content. The IL content improves the number of charge carriers whereas temperature improves the intrachain ion mobility and dissociation of IL, favoring the inter-chain hopping and enhancing ionic conductivity value [47, 59].

PVDF/IL electrospun membranes show a conductivity value more than 2 orders of magnitude higher than that exhibited by the pristine PVDF membranes. This fact is due to the increase in the ionic charge content within the polymer matrix. Thus, the ionic conductivity value increases when the IL content increases (Figure 4a), as demonstrated for the [Emim][TFSI]/PVDF membranes [47].

The increase in ionic conductivity with temperature is associated to a hopping conduction mechanism between local structural relaxations and segmental motions of polymer salt complexes. As temperature increases, the IL viscosity is reduced and the polymer chains acquire faster internal modes in which bond rotations produce intra-chain ion movements that will increase the IL conductivity [60].

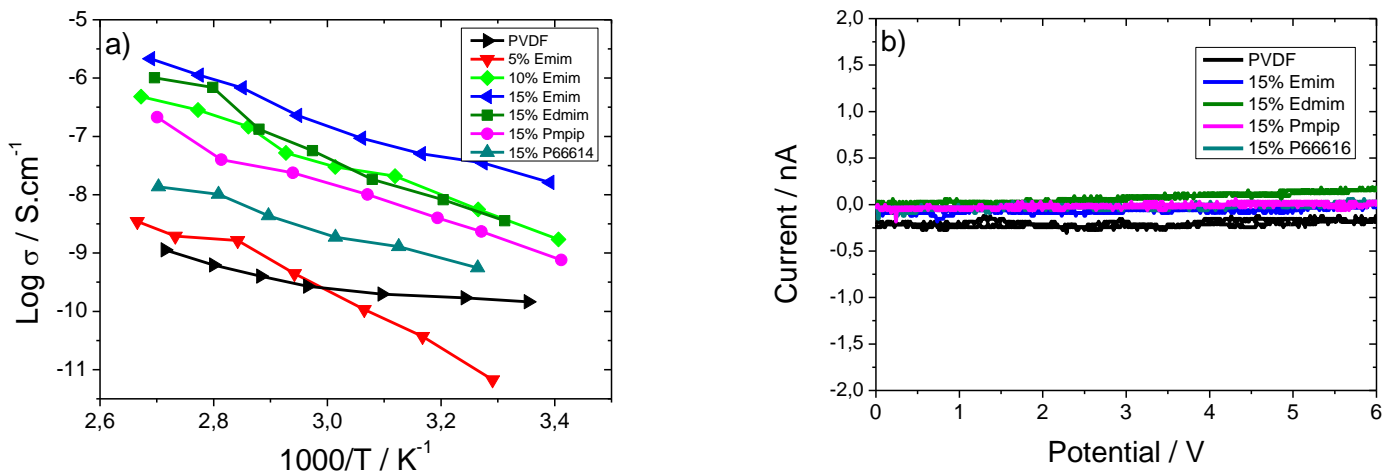


**Figure 4** – a) Ionic conductivity as a function of temperature and b) electrochemical stability of the electrospun membranes.

The temperature ( $T$ ) dependence of the conductivity is described by the Arrhenius equation in the measured range:

$$\sigma = \sigma_0 e^{(-E_a/RT)} \quad (4)$$

where  $E_a$  is the apparent activation energy,  $R$  is the gas constant ( $8.314 \text{ J.mol}^{-1}.\text{K}^{-1}$ ) and  $\sigma_0$  is a pre-exponential factor. The apparent activation energy was calculated through the slope of temperature dependence of the ionic conductivity as is represented in figure 4a.

Table 2 shows the ionic conductivity value at  $25 \text{ }^\circ\text{C}$  and the activation energy of all electrospun membranes, where the electrospun membrane with the highest ionic conductivity value is the PVDF/[Emim][TFSI] with 15 wt.% ( $2 \times 10^{-8} \text{ S.cm}^{-1}$ ).

**Table 2** – Ionic conductivity value at  $25 \text{ }^\circ\text{C}$  and apparent activation energy obtained from equation 1 and 4, respectively for all electrospun membranes.

IL cation	$\sigma_i / \text{S.cm}^{-1}$ at $25 \text{ }^\circ\text{C}$ ( $\pm 3\%$ )	$E_a / \text{kJ.mol}^{-1}$ ( $\pm 3\%$ )
0%	$7 \times 10^{-13}$	63
5% Emim <sup>+</sup>	$7 \times 10^{-12}$	36
10% Emim <sup>+</sup>	$2 \times 10^{-9}$	28
15% Emim <sup>+</sup>	$2 \times 10^{-8}$	26
15% Edmim <sup>+</sup>	$4 \times 10^{-9}$	35
15% Pmpip <sup>+</sup>	$8 \times 10^{-10}$	27
15% P66614 <sup>+</sup>	$6 \times 10^{-10}$	21

Regarding the activation energy, increasing the amount of [Emim][TFSI] in the polymer matrix decreases its value, which is lower for the 15 wt.% sample. For the same amount of IL (15 wt.%), the ionic liquid properties (molecular weight and viscosity) affect this value, with the higher amount of ions in the electrospun membranes decreasing the energy barrier for ion transport [47].

Cyclic voltammetry was used to evaluate the electrochemical stability of the samples, an essential parameter to ensure a good battery performance. Figure 4b shows the cyclic voltammogram curves for the pristine PVDF and 15 wt.% PVDF/IL membranes in the

potential range from 0.0 to 6.0 V (vs. Li/Li<sup>+</sup>) at a scan rate of 10 mV.s<sup>-1</sup> on a gold working electrode at 25 °C. The pristine PVDF membrane shows a stable electrochemical behavior at the considered potential [61]. An electrochemical window stability between ~0.0 and 6.0 V (vs. Li/Li<sup>+</sup>) was observed for all PVDF/IL composites.

Considering the voltage range of certain cathodes, such as LiNiCoMnO<sub>2</sub>, LiMn<sub>2</sub>O<sub>4</sub> and C-LiFePO<sub>4</sub>, the evaluated ionic liquids can be used in LIBs applications due to the high ionic conductivity value and good electrochemical stability.

### *3.4. Cycling performance*

The obtained electrospun membranes show an enhanced ion-dipole interaction, the ion dynamics increasing when compared to the pristine electrospun membranes, which is an advantage for LIBs.

To obtain LIBs with good electrochemical performance in terms of capacity value and electrochemical stability, an ionic conductivity value of at least 10<sup>-4</sup> S.cm<sup>-1</sup> is required. Taking into account this fact and the values presented in table 2, the various electrospun membranes were immersed in the electrolyte solution and tested in batteries. The electrolyte uptake and ionic conductivity value of the PVDF/IL membranes after the uptake process are shown in the supplementary information (Figure S3), leading to ionic conductivity values above 0.5 mS.cm<sup>-1</sup>. Since the pristine PVDF sample presents similar ionic conductivity and charge/discharge behavior when compared to 5 wt.% [Emim][TFSI], only the results for electrospun membranes doped with IL are shown in Figure 5a.

For Li/LiFePO<sub>4</sub> half-cells prepared with the electrospun membrane with 15 wt.% of [Emim][TFSI], Figure 5a shows the 5<sup>th</sup> curve of charge-discharge voltage curves at C/8, C/5, C/2, C and 2C, between 2.5 and 4.2 V. Figure 5a displays the typical flat voltage

plateau around 3.2-3.6 V that indicates the presence of a two-phase  $\text{Fe}^{2+}/\text{Fe}^{3+}$  redox reaction between  $\text{FePO}_4^-$  and  $\text{LiFePO}_4$ , the plateau being independent of the scan rate and cycling number [62]. The flat voltage plateau is detected for scan rates up to C/2 and for scan rates of C and 2C, an oblique line is distinguished that represents a capacitive behavior (Figure 5a) [63].

In addition, Figure 5a) shows that the charge-discharge curves decrease with increasing C-rate due to the influence of ionic transport on the ohmic polarization, but also on the interfacial reaction resistance on the lithium electrode [64]. This fact is also observed for the other electrospun membranes. Figure 5b shows the charge-discharge curves at C rate for the 5<sup>th</sup> cycle for all electrospun membranes, showing that the charge-discharge value is proportional to the ionic conductivity value for each electrospun membranes (Figure S4). Figure 5c shows the discharge capacity value as a function of the number of cycles for all electrospun membranes from C/8 to 2C. For all electrospun membranes, excepting for the membrane with 5% of [Emim][TFSI] up to C-rate, the discharge capacity is very stable as a function of the cycle number. The differences observed in the cycling behavior are related to the different ionic conductivity values of the IL and to the variations in the membrane uptake percentage value, both leading to a different ionic conductivity of the electrospun membranes with the electrolyte. The low ionic conductivity and low IL content lead to a low discharge capacity.

At C-rate, electrospun membranes with 15 wt.% IL content led to discharge capacity values of 119, 118, 104, and 95  $\text{mAh}\cdot\text{g}^{-1}$  for  $[\text{Emim}]^+$ ,  $[\text{P66614}]^+$ ,  $[\text{Edmim}]^+$  and  $[\text{Pmpip}]^+$ , respectively, indicating excellent electrochemical behavior.

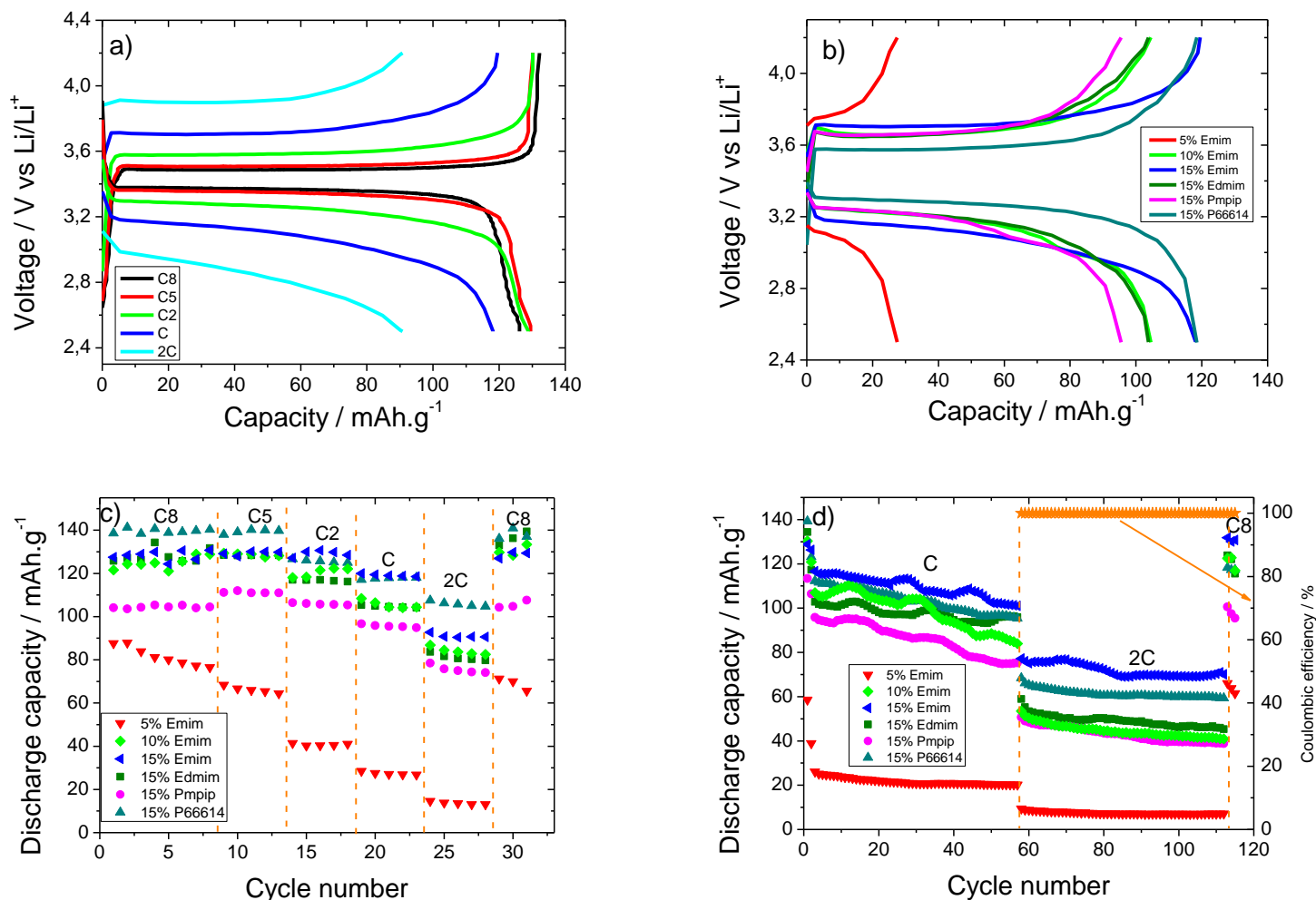


**Figure 5** – a) 5th charge and discharge room temperature cycle profiles at rates from C/5 to 5C for electrospun membranes with 15 wt.% of [Emim][TFSI], b) 5th cycle of charge and discharge at C-rate for all electrospun membranes, c) rate performance as a function of the cycling number and d) cycle life at C and 2C, for all electrospun membranes.

Considering the excellent electrochemical results represented in Figure 5c, Figure 5d shows the discharge capacity of the different membranes at C- and 2C-rates for 50 cycles. For these high scan-rates, good cycling stability as a function of the cycle number is observed. The sample with the best cycling behavior is the electrospun membrane with 15 wt.% of [Emim][TFSI], which after 50 cycles at 2C-rate exhibits 70 mAh.g<sup>-1</sup> and a capacity fade < 3%. Furthermore, all electrospun membranes reveal excellent reversibility of the process, since the coulombic efficiency (CE) is ~ 100% (Figure 5d).

In order to better understand the electrochemical performance of the cathodic half-cells assembled with the electrospun membranes, the EIS spectra of the half-cells were recorded before and after cycling, as shown in the Nyquist plot reproduced in Figure 6. Figure 6a represents the Nyquist plots for all electrospun membranes obtained before cycling. Nyquist plots are characterized by a semicircle (representing the overall resistance, which is the sum of the ohmic resistance, that represents the contact film resistance, and resistance contributions from the charge-transfer reaction resistance) in the high and medium frequency regions, and a straight line that is associated to the  $\text{Li}^+$  diffusion process in the low frequency region. This behavior is also similar for all electrospun membranes after cycling, as it is demonstrated in Figure 6b, being the main difference the variation of the overall resistance.

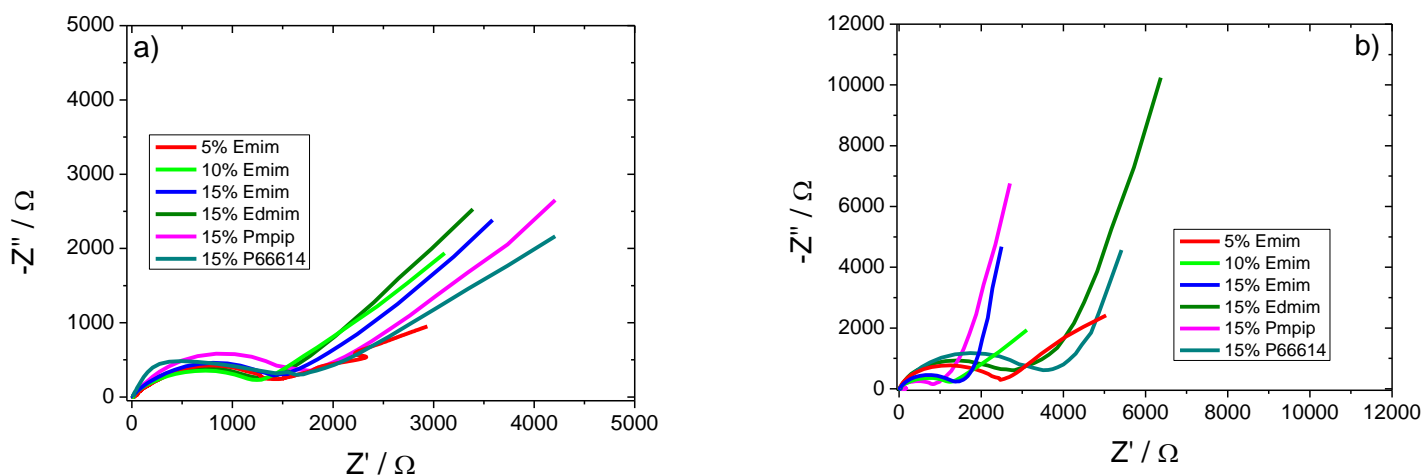


**Figure 6** – Impedance spectroscopy of the cathodic half-cells for different electrospun membranes a) before and b) after cycling.

The overall resistance values for the different electrospun membranes before and after cycling were obtained by impedance spectroscopy and are shown in Table 3

**Table 3** – Overall resistance before and after cycling for the different electrospun membranes.

IL cation	R <sub>s</sub> / Ω	
	Before cycling	After cycling
5% Emim	1432	2438
10% Emim	1240	1200
15% Emim	1474	1418
15% Edmim	1352	2700
15% Pmpip	1750	850
15% P66614	1542	3700

The overall resistance of the electrospun membranes containing 5 wt.% of [Emim]<sup>+</sup>, 15 wt.% of [Edmim]<sup>+</sup> and 15 wt.% of [P66614]<sup>+</sup> increases due to the formation of a solid electrolyte interface (SEI) layer during cycling [65]. For high amounts (10 and 15 wt.%) of [Emim]<sup>+</sup> and [Pmpip]<sup>+</sup>, the presence of IL reduces the SEI layer formation, which results in an improvement of the interface between the separator and the electrode.

Considering the excellent charge-discharge results presented in Figure 5, Table 4 compares the electrochemical properties of the electrospun membranes obtained in this work with other electrospun membranes reported in the literature for the same electrode.

**Table 4** –Ionic conductivity and discharge capacity for different electrospun membranes reported in the literature for C-LiFePO<sub>4</sub> cathodes.

Polymer matrix	Fillers	Electrolyte	Porosity /Uptake (%)	Ionic conductivity (S/cm)	Discharge capacity (mAh/g)	Ref
Cellulose	HNT	LiPF <sub>6</sub>	86.3/311	1.36E-3	125.31 (1C)	[66]
FPEEK	-	LiPF <sub>6</sub> (EMC/DMC/ EC 1:1:1 v/v/v)	88/559	3.12E-3	150.5 (C/2)	[67]
Poly(ethylene oxide)	SiO <sub>2</sub>	LiTFSI, Pyr <sub>14</sub> TFSI	-/-	1E-4 (30°C)	150 (C/5)	[37]
Polyacrylonitrile	-	PYR <sub>13</sub> TFSI	83/-	-	~140 (C/10)	[43]
Polyethylene Carbonate	SiO <sub>2</sub>	LiTFSI, Pyr <sub>14</sub> TFSI	-/-	1E-7 (30°C)	100 (C/15)	[38]
Polyimide	AlOOH	LiPF <sub>6</sub> (EC/DEC 1:1 w/w)	65.8/337.5	2.18E-3	154 (1C)	[68]

Polytetrafluoro ethylene	-	LiPF <sub>6</sub> (EC/DMC 1:1 v/v)	80/325	1.87E-3	142	[69]
Polyurethane	Graphene oxide	LiPF <sub>6</sub> (EC/EMC/DMC) (1/1/1, w/w/w)	90.7/733	3.73E-3	154 (C/5)	[70]
PVA/chitosan	-	EmimCl	-/-	1E-4	-	[71]
PVDF	[Emim][TFSI]	LiPF <sub>6</sub> (EC/DMC 1:1 w/w)	---/4186	3.1E-3	112 (2C)	In this work
PVDF-CTFE	Sb <sub>2</sub> O <sub>3</sub>	LiPF <sub>6</sub> (EC/DEC 1:1 w/w)	72/356	2.88E-3	167 (1C)	[72]
PVDF-HFP	-	LiTFSI, EmimTFSI	58/250	9.9E-3 (25°C)	80 (1C)	[41]
PVDF-HFP	SiO <sub>2</sub> PPTFSI	-	83/552	6.4E-4	119 (1C)	[44]
PVDF-HFP	PMIA	-	-/-	1.21E-3	153.8 (C/2)	[73]
PVDF-HFP/PPEGMA	-	BMITFSI, LiTFSI	87/420	2.3E-3 (25°C)	125 (1C)	[42]
PVDF-TrFE	Al <sub>2</sub> O <sub>3</sub>	LiPF <sub>6</sub> (EC/DMC 1:1 v/v)	80/375	5.8E-3 (25°C)	154 (C/10)	[29]

Table 4 demonstrates that the electrochemical results of the present work are similar or even better than those reported in the literature for other electrospun membranes. Thus, taking into account the ionic conductivity value and the excellent electrochemical behavior of the PVDF/[Emim][TFSI] membrane, it is concluded that the addition of ILs leads to electrospun functional membranes with improved ionic conductivity, and good thermal and mechanical stability, allowing improved battery performance, particularly at higher scan rates.

The novel electrospun membranes presented in this work can be successfully used as separators, where the addition of IL increases the electrochemical properties, and the cation type plays a relevant role for lithium ion battery applications.



#### 4. Conclusions

PVDF electrospun fiber membranes with different contents of ILs sharing the same anion [TFSI]<sup>-</sup> were obtained. Independently of the IL cation type, the fiber diameter decreased due to the presence of ionic charges in the solution. Although the PVDF fibers show a high  $\beta$  phase content, mainly due to the room temperature solvent evaporation, the incorporation of high IL contents does not, however, have a significant influence on this value. The thermal stability and degree of crystallinity are reduced in the presence of IL within the PVDF matrix, which is caused by the strong electrostatic interactions between the IL and the highly polar polymer chains. Impedance spectroscopy analysis allowed the determination of the ionic conductivity, with a maximum of  $2.8 \text{ mS.cm}^{-1}$  at room temperature for 15 wt.% [Emim][TFSI]. All electrospun membranes showed electrochemical stability in the voltage range of 0.0 to 6.0 V and the assembled battery half-cells presented good performances, reaching a maximum discharge capacity of  $119 \text{ mAh.g}^{-1}$  at C-rate, and a 100% of coulombic efficiency. The results reported here prove the applicability of electrospun PVDF/IL membranes in the production of separator membranes for LIB applications.

#### Acknowledgements

Work supported by the Portuguese Foundation for Science and Technology (FCT): projects UID/FIS/04650/2019, UID/QUI/0686/2019, UID/CTM/50025/2019, UID/QUI/50006/2019, UID/QUI/00686/2016, UID/QUI/00686/2018, PTDC/FIS-MAC/28157/2017, and Grants SFRH/BD/140842/2018 (J.C.B.), SFRH/BPD/121526/2016 (D.M.C), CEECIND/00833/2017 (R.G.) and SFRH/BPD/112547/2015 (C.M.C.). Financial support from the Spanish State Research Agency (AEI) and the European Regional Development Fund (ERFD) through the project PID2019-106099RB-C43/AEI/10.13039/501100011033 and from the Basque

Government Industry and Education Departments under the ELKARTEK and HAZITEK programs is also acknowledged.

## References

- [1] B. Scrosati, J. Garche, Lithium batteries: Status, prospects and future, *Journal of Power Sources*, 195 (2010) 2419-2430.
- [2] B. Scrosati, J. Hassoun, Y.K. Sun, Lithium-ion batteries. A look into the future, *Energy & Environmental Science*, 4 (2011) 3287-3295.
- [3] K.M. Abraham, Prospects and Limits of Energy Storage in Batteries, *The journal of physical chemistry letters*, 6 (2015) 830-844.
- [4] M.S. Whittingham, Lithium Batteries and Cathode Materials, *Chemical Reviews*, 104 (2004) 4271-4302.
- [5] P. Arora, Z. Zhang, Battery Separators, *Chemical Reviews*, 104 (2004) 4419-4462.
- [6] A. Arya, M. Sadiq, A.L. Sharma, Effect of variation of different nanofillers on structural, electrical, dielectric, and transport properties of blend polymer nanocomposites, *Ionics*, 24 (2017) 2295-2319.
- [7] X. Li, Z.J. Wang, H. Lin, Y.D. Liu, Y. Min, F. Pan, Composite electrolytes of pyrrolidone-derivatives-PEO enable to enhance performance of all solid state lithium-ion batteries, *Electrochimica Acta*, 293 (2019) 25-29.
- [8] B. Liu, Y. Huang, H. Cao, L. Zhao, Y. Huang, A. Song, Y. Lin, M. Wang, X. Li, A novel polyacrylonitrile-based porous structure gel polymer electrolyte composited by incorporating polyhedral oligomeric silsesquioxane by phase inversion method, *Journal of Solid State Electrochemistry*, 22 (2018) 1771-1783.
- [9] J. Bao, X. Qu, G. Qi, Q. Huang, S. Wu, C. Tao, M. Gao, C. Chen, Solid electrolyte based on waterborne polyurethane and poly(ethylene oxide) blend polymer for all-solid-state lithium ion batteries, *Solid State Ionics*, 320 (2018) 55-63.
- [10] K. Yang, Z. Zhang, Z. Liao, L. Yang, S.-i. Hirano, Organic Ionic Plastic Crystal-polymer Solid Electrolytes with High Ionic Conductivity and Mechanical Ability for Solid-state Lithium Ion Batteries, *ChemistrySelect*, 3 (2018) 12595-12599.
- [11] F. Pignanelli, M. Romero, M. Esteves, L. Fernández-Werner, R. Faccio, A.W. Mombrú, Lithium titanate nanotubes as active fillers for lithium-ion polyacrylonitrile solid polymer electrolytes, *Ionics*, (2018).

- [12] M.V. Bhute, S.B. Kondawar, P. Koinkar, Fabrication of hybrid gel nanofibrous polymer electrolyte for lithium ion battery, *International Journal of Modern Physics B*, 32 (2018) 1840066.
- [13] Y. Liu, X. Ma, K. Sun, K. Yang, F. Chen, Preparation and characterization of gel polymer electrolyte based on electrospun polyhedral oligomeric silsesquioxane-poly(methyl methacrylate)/polyvinylidene fluoride hybrid nanofiber membranes for lithium-ion batteries, *Journal of Solid State Electrochemistry*, 22 (2017) 581-590.
- [14] X. Shi, N. Ma, Y. Wu, Y. Lu, Q. Xiao, Z. Li, G. Lei, Fabrication and electrochemical properties of LATP/PVDF composite electrolytes for rechargeable lithium-ion battery, *Solid State Ionics*, 325 (2018) 112-119.
- [15] J.C. Barbosa, J.P. Dias, S. Lancers-Mendez, C.M. Costa, Recent Advances in Poly(vinylidene fluoride) and Its Copolymers for Lithium-Ion Battery Separators, Membranes (Basel), 8 (2018).
- [16] S. Choudhury, S. Stalin, Y. Deng, L.A. Archer, Soft Colloidal Glasses as Solid-State Electrolytes, *Chemistry of Materials*, 30 (2018) 5996-6004.
- [17] D. Li, D. Qin, F. Nie, L. Wen, L. Xue, Enhancement of electrochemical performance of lithium-ion battery by single-ion conducting polymer addition in ceramic-coated separator, *Journal of Materials Science*, 53 (2018) 11038-11049.
- [18] Y. Tsuchida, M. Matsumiya, K. Tsunashima, Preparation of polymer electrolytes using ionic liquids and evaluation of physicochemical properties, *Journal of Molecular Liquids*, 274 (2019) 204-208.
- [19] A. Wang, H. Xu, F. Liu, X. Liu, S. Wang, Q. Zhou, J. Chen, S. Yang, L. Zhang, Polyimide-Based Self-Standing Polymer Electrolyte Membrane for Lithium-Ion Batteries, *Energy Technology*, 6 (2018) 326-332.
- [20] G. Yang, B. Fan, F. Liu, F. Yao, Q. Wang, Ion Pair Integrated Organic-Inorganic Hybrid Electrolyte Network for Solid-State Lithium Ion Batteries, *Energy Technology*, 6 (2018) 2319-2325.
- [21] M. Watanabe, M.L. Thomas, S. Zhang, K. Ueno, T. Yasuda, K. Dokko, Application of Ionic Liquids to Energy Storage and Conversion Materials and Devices, *Chem Rev*, 117 (2017) 7190-7239.
- [22] S.K. Singh, Shalu, L. Balo, H. Gupta, V.K. Singh, A.K. Tripathi, Y.L. Verma, R.K. Singh, Improved electrochemical performance of EMIMFSI ionic liquid based gel polymer electrolyte with temperature for rechargeable lithium battery, *Energy*, 150 (2018) 890-900.

- [23] M. Li, Y. Liao, Q. Liu, J. Xu, P. Sun, H. Shi, W. Li, Application of the imidazolium ionic liquid based nano-particle decorated gel polymer electrolyte for high safety lithium ion battery, *Electrochimica Acta*, 284 (2018) 188-201.
- [24] G.T. Kim, S. Passerini, M. Carewska, G.B. Appetecchi, Ionic Liquid-Based Electrolyte Membranes for Medium-High Temperature Lithium Polymer Batteries, *Membranes (Basel)*, 8 (2018).
- [25] J.-K. Kim, Influence of ionic liquid structures on polyimide-based gel polymer electrolytes for high-safety lithium batteries, *Journal of Industrial and Engineering Chemistry*, 68 (2018) 168-172.
- [26] J.H. Lin, Y.F. Huang, H.W. Wu, J.H. Li, Y.T. Zeng, Electrospun PVDF-HFP/BR Rubber Composites for High Performance Solid State Electrolytes, *Materials Science Forum*, 909 (2017) 163-168.
- [27] S.-X. Wang, C.C. Yap, J. He, C. Chen, S.Y. Wong, X. Li, Electrospinning: a facile technique for fabricating functional nanofibers for environmental applications, *Nanotechnology Reviews*, 5 (2016).
- [28] Y. Li, Q. Li, Z. Tan, A review of electrospun nanofiber-based separators for rechargeable lithium-ion batteries, *Journal of Power Sources*, 443 (2019) 227262.
- [29] B. K. S. Suriyakumar, A.P. P. A. A. S, N. Kalarikkal, A.M. Stephen, G.V. G, D. Rouxel, S. Thomas, Highly lithium ion conductive, Al<sub>2</sub>O<sub>3</sub> decorated electrospun P(VDF-TrFE) membranes for lithium ion battery separators, *New Journal of Chemistry*, 42 (2018) 19505-19520.
- [30] M. Zhao, J. Wang, C. Chong, X. Yu, L. Wang, Z. Shi, An electrospun lignin/polyacrylonitrile nonwoven composite separator with high porosity and thermal stability for lithium-ion batteries, *RSC Advances*, 5 (2015) 101115-101120.
- [31] C. Fang, S. Yang, X. Zhao, P. Du, J. Xiong, Electrospun montmorillonite modified poly(vinylidene fluoride) nanocomposite separators for lithium-ion batteries, *Materials Research Bulletin*, 79 (2016) 1-7.
- [32] Y. Wang, S. Wang, J. Fang, L.-X. Ding, H. Wang, A nano-silica modified polyimide nanofiber separator with enhanced thermal and wetting properties for high safety lithium-ion batteries, *Journal of Membrane Science*, 537 (2017) 248-254.
- [33] M. Yanilmaz, J. Zhu, Y. Lu, H. Jiang, X. Zhang, High-strength, thermally stable nylon 6,6 composite nanofiber separators for lithium-ion batteries, *Journal of Materials Science*, 52 (2017).

- [34] J. Shayapat, O.H. Chung, J.S. Park, Electrospun polyimide-composite separator for lithium-ion batteries, *Electrochimica Acta*, 170 (2015) 110-121.
- [35] Y. Liang, L. Ji, B. Guo, Z. Lin, Y. Yao, Y. Li, M. Alcoutlabi, Y. Qiu, X. Zhang, Preparation and electrochemical characterization of ionic-conducting lithium lanthanum titanate oxide/polyacrylonitrile submicron composite fiber-based lithium-ion battery separators, *Journal of Power Sources*, 196 (2011) 436-441.
- [36] Y. Liang, Z. Lin, Y. Qiu, X. Zhang, Fabrication and characterization of LATP/PAN composite fiber-based lithium-ion battery separators, *Electrochimica Acta*, 56 (2011) 6474-6480.
- [37] Y.T. Kento Kimura, Ionic Liquid-Containing Composite Poly(ethylene oxide) Electrolyte Reinforced by Electrospun Silica Nanofiber, *Journal of The Electrochemical Society*, 164 (2017) 3357-3361.
- [38] K. Kimura, H. Matsumoto, J. Hassoun, S. Panero, B. Scrosati, Y. Tominaga, A Quaternary Poly(ethylene carbonate)-Lithium Bis(trifluoromethanesulfonyl)imide-Ionic Liquid-Silica Fiber Composite Polymer Electrolyte for Lithium Batteries, *Electrochimica Acta*, 175 (2015) 134-140.
- [39] M.A. Navarra, L. Lombardo, P. Bruni, L. Morelli, A. Tsurumaki, S. Panero, F. Croce, Gel Polymer Electrolytes Based on Silica-Added Poly(ethylene oxide) Electrospun Membranes for Lithium Batteries, *Membranes (Basel)*, 8 (2018).
- [40] J.-K. Kim, Hybrid gel polymer electrolyte for high-safety lithium-sulfur batteries, *Materials Letters*, 187 (2017) 40-43.
- [41] K. Kim, J.-K. Kim, Organic di-radical rechargeable battery with an ionic liquid-based gel polymer electrolyte, *Korean Journal of Chemical Engineering*, 33 (2016) 858-861.
- [42] Y. Tong, M. Que, S. Su, L. Chen, Design of amphiphilic poly(vinylidene fluoride-co-hexafluoropropylene)-based gel electrolytes for high-performance lithium-ion batteries, *Ionics*, 22 (2016) 1311-1318.
- [43] T. Evans, J.-H. Lee, V. Bhat, S.-H. Lee, Electrospun polyacrylonitrile microfiber separators for ionic liquid electrolytes in Li-ion batteries, *Journal of Power Sources*, 292 (2015) 1-6.
- [44] Y. Cheng, L. Zhang, S. Xu, H. Zhang, B. Ren, T. Li, S. Zhang, Ionic liquid functionalized electrospun gel polymer electrolyte for use in a high-performance lithium metal battery, *Journal of Materials Chemistry A*, 6 (2018) 18479-18487.

- [45] H. Matsumoto, Recent Advances in Ionic Liquids for Lithium Secondary Batteries, in: T.R. Jow, K. Xu, O. Borodin, M. Ue (Eds.) *Electrolytes for Lithium and Lithium-Ion Batteries*, Springer New York, New York, NY, 2014, pp. 209-225.
- [46] C. Ribeiro, C.M. Costa, D.M. Correia, J. Nunes-Pereira, J. Oliveira, P. Martins, R. Goncalves, V.F. Cardoso, S. Lancers-Mendez, Electroactive poly(vinylidene fluoride)-based structures for advanced applications, *Nat Protoc*, 13 (2018) 681-704.
- [47] R. Leones, C.M. Costa, A.V. Machado, J.M.S.S. Esperança, M.M. Silva, S. Lancers-Méndez, Effect of Ionic Liquid Anion Type in the Performance of Solid Polymer Electrolytes Based on Poly(Vinylidene fluoride-trifluoroethylene), *Electroanalysis*, 27 (2015) 457-464.
- [48] A. Gören, J. Mendes, H.M. Rodrigues, R.E. Sousa, J. Oliveira, L. Hilliou, C.M. Costa, M.M. Silva, S. Lancers-Méndez, High performance screen-printed electrodes prepared by a green solvent approach for lithium-ion batteries, *J Power Sources*, 334 (2016) 65-77.
- [49] J.C. Dias, D.C. Correia, A.C. Lopes, S. Ribeiro, C. Ribeiro, V. Sencadas, G. Botelho, J.M.S.S. Esperança, J.M. Laza, J.L. Vilas, L.M. León, S. Lancers-Méndez, Development of poly(vinylidene fluoride)/ionic liquid electrospun fibers for tissue engineering applications, *Journal of Materials Science*, 51 (2016) 4442-4450.
- [50] D.M. Correia, J.C. Barbosa, C.M. Costa, P.M. Reis, J.M.S.S. Esperança, V. de Zea Bermudez, S. Lancers-Méndez, Ionic Liquid Cation Size-Dependent Electromechanical Response of Ionic Liquid/Poly(vinylidene fluoride)-Based Soft Actuators, *The Journal of Physical Chemistry C*, 123 (2019) 12744-12752.
- [51] P. Martins, A.C. Lopes, S. Lancers-Mendez, Electroactive phases of poly(vinylidene fluoride): Determination, processing and applications, *Progress in Polymer Science*, 39 (2014) 683-706.
- [52] J.C. Dias, D.M. Correia, C.M. Costa, C. Ribeiro, A. Maceiras, J.L. Vilas, G. Botelho, V. de Zea Bermudez, S. Lancers-Mendez, Improved response of ionic liquid-based bending actuators by tailored interaction with the polar fluorinated polymer matrix, *Electrochimica Acta*, 296 (2019) 598-607.
- [53] M. Herstedt, M. Smirnov, P. Johansson, M. Chami, J. Grondin, L. Servant, J.C. Lassègues, Spectroscopic characterization of the conformational states of the bis(trifluoromethanesulfonyl)imide anion (TFSI<sup>-</sup>), *Journal of Raman Spectroscopy*, 36 (2005) 762-770.

- [54] A. Roy, B. Dutta, S. Bhattacharya, Electroactive phase nucleation and non-isothermal crystallization kinetics study in [DEMM][TFSI] ionic liquid incorporated P(VDF-HFP) co-polymer membranes, *Journal of Materials Science*, 51 (2016) 7814-7830.
- [55] M. Kundu, C.M. Costa, J. Dias, A. Maceiras, J.L. Vilas, S. Lanceros-Méndez, On the Relevance of the Polar  $\beta$ -Phase of Poly(vinylidene fluoride) for High Performance Lithium-Ion Battery Separators, *The Journal of Physical Chemistry C*, 121 (2017) 26216-26225.
- [56] A. Reizabal, R. Gonçalves, A. Fidalgo-Marijuan, C.M. Costa, L. Pérez, J.-L. Vilas, S. Lanceros-Mendez, Tailoring silk fibroin separator membranes pore size for improving performance of lithium ion batteries, *Journal of Membrane Science*, 598 (2020) 117678.
- [57] M. Park, X. Zhang, M. Chung, G.B. Less, A.M. Sastry, A review of conduction phenomena in Li-ion batteries, *J Power Sources*, 195 (2010) 7904-7929.
- [58] Y. Zhu, S. Xiao, Y. Shi, Y. Yang, Y. Wu, A trilayer poly(vinylidene fluoride)/polyborate/poly(vinylidene fluoride) gel polymer electrolyte with good performance for lithium ion batteries, *Journal of Materials Chemistry A*, 1 (2013) 7790-7797.
- [59] N. Wongittharom, T.-C. Lee, C.-H. Hsu, G. Ting-Kuo Fey, K.-P. Huang, J.-K. Chang, Electrochemical performance of rechargeable Li/LiFePO<sub>4</sub> cells with ionic liquid electrolyte: Effects of Li salt at 25 °C and 50 °C, *J Power Sources*, 240 (2013) 676-682.
- [60] M.M. Silva, P.C. Barbosa, L.C. Rodrigues, A. Gonçalves, C. Costa, E. Fortunato, Gelatin in electrochromic devices, *Optical Materials*, 32 (2010) 719-722.
- [61] S. Janakiraman, A. Surendran, S. Ghosh, S. Anandhan, A. Venimadhav, Electroactive poly(vinylidene fluoride) fluoride separator for sodium ion battery with high coulombic efficiency, *Solid State Ionics*, 292 (2016) 130-135.
- [62] Y.-H. Nien, J.R. Carey, J.-S. Chen, Physical and electrochemical properties of LiFePO<sub>4</sub>/C composite cathode prepared from various polymer-containing precursors, *J Power Sources*, 193 (2009) 822-827.
- [63] S.-X. Zhao, H. Ding, Y.-C. Wang, B.-H. Li, C.-W. Nan, Improving rate performance of LiFePO<sub>4</sub> cathode materials by hybrid coating of nano-Li<sub>3</sub>PO<sub>4</sub> and carbon, *Journal of Alloys and Compounds*, 566 (2013) 206-211.
- [64] W. Xiao, L. Zhao, Y. Gong, S. Wang, J. Liu, C. Yan, Preparation of high performance lithium-ion batteries with a separator-cathode assembly, *RSC Advances*, 5 (2015) 34184-34190.

- [65] J. Guo, A. Sun, X. Chen, C. Wang, A. Manivannan, Cyclability study of silicon-carbon composite anodes for lithium-ion batteries using electrochemical impedance spectroscopy, *Electrochim Acta*, 56 (2011) 3981-3987.
- [66] S. Wang, D. Zhang, Z. Shao, S. Liu, Cellulosic materials-enhanced sandwich structure-like separator via electrospinning towards safer lithium-ion battery, *Carbohydrate Polymers*, 214 (2019) 328-336.
- [67] H. Li, B. Zhang, W. Liu, B. Lin, Q. Ou, H. Wang, M. Fang, D. Liu, S. Neelakandan, L. Wang, Effects of an electrospun fluorinated poly(ether ether ketone) separator on the enhanced safety and electrochemical properties of lithium ion batteries, *Electrochimica Acta*, 290 (2018) 150-164.
- [68] G. Zhong, Y. Wang, C. Wang, Z. Wang, S. Guo, L. Wang, X. Liang, H. Xiang, An AlOOH-coated polyimide electrospun fibrous membrane as a high-safety lithium-ion battery separator, *Ionics*, (2018).
- [69] J. Li, Q. Zhong, Y. Yao, S. Bi, T. Zhou, X. Guo, M. Wu, T. Feng, R. Xiang, Electrochemical performance and thermal stability of the electrospun PTFE nanofiber separator for lithium-ion batteries, *Journal of Applied Polymer Science*, 135 (2018) 46508.
- [70] X. Liu, K. Song, C. Lu, Y. Huang, X. Duan, S. Li, Y. Ding, Electrospun PU@GO separators for advanced lithium ion batteries, *Journal of Membrane Science*, 555 (2018) 1-6.
- [71] R.S. Datta, S.M. Said, S.R. Shahrir, N. Abdullah, M.F.M. Sabri, S. Balamurugan, Y. Miyazaki, K. Hayashi, N.A. Hashim, U. Habiba, A.M. Afifi, Ionic liquid entrapment by an electrospun polymer nanofiber matrix as a high conductivity polymer electrolyte, *RSC Advances*, 5 (2015) 48217-48223.
- [72] L. Wang, Z. Wang, Y. Sun, X. Liang, H. Xiang, Sb<sub>2</sub>O<sub>3</sub> modified PVDF-CTFE electrospun fibrous membrane as a safe lithium-ion battery separator, *Journal of Membrane Science*, 572 (2019) 512-519.
- [73] H. Zhao, N. Deng, J. Ju, Z. Li, W. Kang, B. Cheng, Novel configuration of heat-resistant gel polymer electrolyte with electrospun poly (vinylidene fluoride-co-hexafluoropropylene) and poly-m-phenyleneisophthalamide composite separator for high-safety lithium-ion battery, *Materials Letters*, 236 (2019) 101-105.